Three-Dimensional Variational Analysis with Spatially Inhomogeneous Covariances

WAN-SHU WU AND R. JAMES PURSER

Science Applications International Corp., Beltsville, Maryland

DAVID F. PARRISH

National Centers for Environmental Prediction, Environmental Modeling Center, Washington, D.C.

(Manuscript received 1 February 2002, in final form 17 May 2002)

ABSTRACT

In this study, a global three-dimensional variational analysis system is formulated in model grid space. This formulation allows greater flexibility (e.g., inhomogeneity and anisotropy) for background error statistics. A simpler formulation, inhomogeneous only in the latitude direction, was chosen for these initial tests. The background error statistics are defined as functions of the latitudinal grid and are estimated with the National Meteorological Center (NMC) method. The horizontal scales of the variables are obtained through the variances of the variables and of their Laplacian. The vertical scales are estimated through the statistics of the vertical correlation of each variable and are applied locally using recursive filters. For the multivariate correlation between wind and mass fields, a statistical linear relationship between the streamfunction and the balanced part of temperature and surface pressure is assumed. A localized correlation between the velocity potential and the streamfunction is also used to account for the positive correlation between the vorticity and divergence in the planetary boundary layer.

Horizontally, the global domain is divided into three pieces so that efficient spatial recursive filters can be used to spread out the information from the observation locations. This analysis system is tested against the operational Spectral Statistical-Interpolation analysis system used at the National Centers for Environmental Prediction. The results indicate that 3DVAR in physical space is as effective as 3DVAR in spectral space in the extratropics and yields superior results in the Tropics as a result of the latitude dependence of the background error statistics.

1. Introduction

Current implementations of three-dimensional variational analysis (3DVAR) at many operational centers are constructed in spectral space, which has the advantage that the statistics of background error, both structure and amplitude, can be easily obtained and applied in the analysis procedure. It is simpler to apply a diagonal background error covariance in spectral space than to convolve the corresponding smoothing kernel with the innovations in physical space. However, with only a diagonal covariance in spectral space, the structure function is limited to being geographically homogeneous and isotropic about its center (Parrish and Derber 1992; Courtier et al. 1998). One has little control over the spatial variation of the error statistics when a simplified diagonal background error covariance in spectral space is used. With some computational cost associated with extra transforms in and out of the physical space in each iteration of the optimization solver, spatially inhomogeneous, for example, latitude-dependent, *variances* can be applied. But, it is not as easy to construct inhomogeneous and/or anisotropic *shapes for the covariance profiles* in spectral space. Other methods have been tested for inhomogeneous and/or anisotropic covariance, for example, Derber and Rosati (1989), Desrozier (1997), Riishojgaard (1998), Weaver and Courtier (2001).

Hayden and Purser (1995), extending the work of Purser and McQuigg (1982), showed how a very simple and computationally inexpensive family of recursive filters can be combined to yield empirical smoothers, which are locally isotropic but retain the freedom of spatial inhomogeneity. Recent developments with spatially recursive filters (Purser et al. 2002a, manuscript submitted to *Mon. Wea. Rev.*, hereafter referred to as PWP02a) enable the construction of a variational analysis in physical space, which allows more degrees of freedom in defining the error statistics adaptively. The final goal is to have an analysis system with inhomogeneous and generally anisotropic three-dimensional background error covariances.

In this paper we test and illustrate the first step toward this goal; a global 3DVAR in physical space that is as

Corresponding author address: Wan-Shu Wu, NOAA/NWS/NCEP, W/NP, Room 207, 5200 Auth Rd., Camp Springs, MD 20746.
E-mail: wanshu.wu@noaa.gov

effective as 3DVAR in spectral space. Using recursive filters, we construct an analysis system in physical space with latitude-dependent structure functions and other error statistics. The background error covariances are still isotropic and homogenous in the zonal direction. The basic structure of the 3DVAR is described in section 2 and aspects of the application of the recursive filters to the global domain in section 3. In section 4 we discuss the method used to estimate the background error statistics. The results and conclusions are presented in sections 5 and 6.

2. Global analysis on grid space

In order to incorporate as much as possible of the existing formulation of the global analysis system at the National Centers for Environmental Prediction (NCEP), the version in physical space is formulated to be similar to the current NCEP spectral version: the Spectral Statistical-Interpolation (SSI) analysis system. Notation used here loosely conforms with that of Ide et al. (1997). The functional to be minimized is

$$J = 1/2\ [\mathbf{x}^{\mathrm{T}}\mathbf{B}^{-1}\mathbf{x} + (\mathbf{Hx} - \mathbf{y})^{\mathrm{T}}\mathbf{R}^{-1}(\mathbf{Hx} - \mathbf{y})] \quad (2.1)$$

where

- $\mathbf{x}$ is a vector of analysis increment,
- $\mathbf{B}$ is the background error covariance matrix,
- $\mathbf{y}$ is a vector of the observational residuals, $\mathbf{y} = \mathbf{y}_{\mathrm{obs}} - \mathbf{Hx}_{\mathrm{guess}}$
- $\mathbf{R}$ is the observational and representativeness error covariance matrix,
- $\mathbf{H}$ is a transformation operator from the analysis variable to the form of the observation vector.

The analysis variables, defined on the grid instead of in spectral coefficients, are: streamfunction (ψ); unbalanced part of velocity potential (χ); the unbalanced part of temperature (T); unbalanced part of surface pressure (P); and pseudo–relative humidity (q) [water vapor mixing ratio divided by the saturated value from the guess field, Dee and Da Silva (2002). Calculation of $\mathbf{H}^{\mathrm{T}}\mathbf{R}^{-1}(\mathbf{Hx} - \mathbf{y})$ involves the following steps:

- Calculate T_b, χ_b, and P_b from the analysis variables ψ and add them to the unbalanced parts.
- Convert ψ and χ to U and V.
- Apply observational forward model on the variables
- Calculate the residual, multiply by $\mathbf{R}^{-1}$.
- Apply the adjoint of the first three steps in the reversed order.

The background error $\mathbf{B}$ can be written as $\mathbf{B}_z(\mathbf{V}^1\mathbf{B}_x^1\mathbf{B}_y^1\mathbf{B}_y^1\mathbf{B}_x^1\mathbf{V}^1 + \mathbf{V}^2\mathbf{B}_x^2\mathbf{B}_y^2\mathbf{B}_y^2\mathbf{B}_x^2\mathbf{V}^2)\mathbf{B}_z$ where $\mathbf{V}^1$ and $\mathbf{V}^2$ are the standard deviations of the error. Here, $\mathbf{B}_x$, $\mathbf{B}_y$, and $\mathbf{B}_z$ are applications of recursive filters in the x, y, and z directions. The values $\mathbf{B}^1$ and $\mathbf{B}^2$ are the filters with different scales (see section 4). The preconditioned conjugate-gradient algorithm (Gill et al. 1981; Navon and Legler 1987; Derber and Rosati 1989) was chosen because the multiple filters in the horizontal direction are easier to implement in this solution algorithm. The amplitudes and scales of the background error are defined as functions of latitude and height.

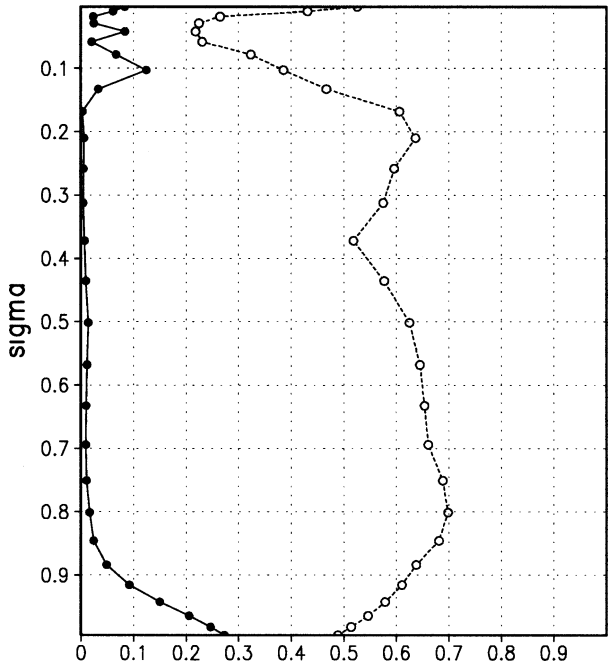

FIG. 1. Global-mean fraction of explained covariance of the balanced part of temperature (open circles) and velocity potential (closed circles).

An initial condition with an appropriate balance between the mass and wind fields minimizes the adjustment and decreases the spinup so that more information from the data can be preserved. The balance also projects information from one analysis variable to the other. For example, over the Southern Ocean where conventional observations are scarce, the mass information from satellite observations is projected in part to the wind field and hence corrects the flow pattern. For 3DVAR in physical space, the multivariate coupling between the analysis variables of mass and wind is a challenge. Since the variables are defined in physical space, it is not easy to apply a linear balance operator (Parrish and Derber 1992) that includes the inverse of the Laplacian operator. However, the relation between the mass field and the streamfunction is linear, so that statistical regression between the two is possible.

The balanced (slow) part of the temperature increment is defined as $T_b = \mathbf{G}\psi$, where matrix $\mathbf{G}$ projects streamfunction increments to a vertical profile of the balanced part of temperature increments. Linear regression is used to calculated the $\mathbf{G}$ matrix. Since the variables are defined on the grid, this matrix can be latitude-dependent. The resulting global means of the fraction of the total temperature and velocity potential explained by the balance relations are shown in Fig. 1. The balanced part of the temperature increments explains from 50% to

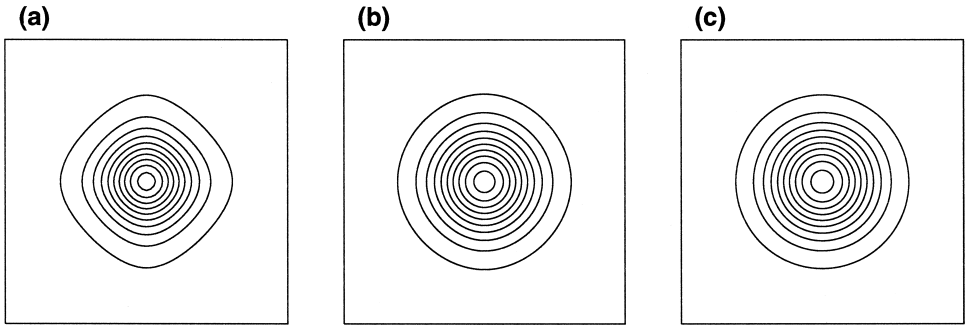

FIG. 2. The results on the Cartesian grid of (a) four applications of first-order recursive filter, (b) one application of fourth-order recursive filter, and (c) the analytical Gaussian.

70% of the variance in the troposphere and decreases to about 20% above 50 mb. The balanced part of the surface pressure increment is defined as $P_b = \mathbf{W}\psi$, where matrix **W** integrates the appropriate contribution of the streamfunction from each level. The balanced part accounts for 86% of the variance of surface pressure increments. A similar balance treatment was also reported in Gustafsson et al. (1999). We find that the balance design is crucial; the assimilation degrades quickly without it. For example, without mass–wind balance the fit of the guess field to the surface pressure observations worsens with time and is doubled in magnitude within 2 days (eight cycles) of the assimilation when compared with the results from the SSI. However, *with* the statistical linear balance defined in the analysis variables, the quality of the first guess field is maintained.

A localized correlation between the velocity potential and the streamfunction is also implemented to take into account the positive correlation between divergence and vorticity in the planetary boundary layer. The balanced part of the velocity potential is defined as $\chi_b = c\psi$, where coefficient c is a function of latitude and height. Shown in Fig. 1, the balanced part explains about 27% of the variance of velocity potential increments near the surface, decreases to a negligible fraction above the boundary layer, and increases again near the tropopause.

3. Application of recursive filters to a global domain

An efficient self-adjoint version of numerical recursive filters can be applied to the task of convolving a spatial distribution of innovations with a smoothing kernel, which is interpreted to be a covariance function of background error. The basic recursive filter involves repetitive smoothing in one direction. Here, we provide a brief summary of the general ideas behind recursive filters, illustrated with the simplest first-order form of this class of filters. For a more technical discussion that includes a description of higher-order forms of the recursive filters, the reader is referred to PWP02a. The simplest first-order smoothing operation consists of an ''advancing'' sweep

$$F_i = (1 - \alpha)D_i + \alpha F_{i-1} \tag{3.1}$$

for increasing index i, where D is the input forcing and F is the result of the sweep, followed by a ''backing'' sweep

$$R_i = (1 - \alpha)F_i + \alpha R_{i+1} \tag{3.2}$$

for decreasing i, where F now represents the input and R the output of the filter. The smoothing parameter α, which lies between 0 and 1, is related to the correlation length of the smoothing response function. The computational advantage of recursive filters over nonrecursive ones can be illustrated by the following example. Assume that $i = 1$, N in (3.1) and the initial forcing is at $i = 1$. Since each F_i depends on the filter result of the previous point F_{i-1}, the result of F_N of the advancing sweep depends on D_1 in just one sweep. On the other hand, it takes $N - 1$ sweeps for the first-order, nonrecursive filters to spread the information from one end of the domain to the other.

Repetitions of this filter produce a quasi-Gaussian response to an initial impulse. The results on the Cartesian grid of (i) four applications of first-order recursive filter, (ii) one application of fourth-order recursive filter, and (iii) the analytical Gaussian, are shown in Figs. 2a,b,c, respectively. The fidelity to a Gaussian form is improved, for a given expenditure of effort, by adopting fewer, but higher-order forms of the filter. The fourth-order recursive filters were used in the experiments reported in this paper. The significance of the Gaussian form of response profile is that, in two dimensions, an isotropic response is obtained by sequentially applying two such filters, once in ''x'' and once in ''y;'' no other profile shape possesses this simplifying property. The computational cost of filtering in two dimensions is simply twice the cost of a one-dimensional application; three-dimensional filters cost only three times as much. In practice, the restriction that covariances should possess only Gaussian profiles is often too severe. However, by linearly superposing two or more Gaussian contributions of different scales and amplitudes, a broader repertoire of isotropic covariance profiles becomes available. The cost increases in proportion to the number

of such contributions, of course. We take up this topic again in section 4.

To use recursive filters in a global variational analysis, there are some basic requirements on the filters. The filters have to be self-adjoint and have the ability to accommodate geographically adaptive horizontal scales. This latter requirement is important not only for generating inhomogeneous structure functions but also for accommodating a nonuniform grid. The recursive filters are also required to have good amplitude control so that the estimated background error variances can be applied precisely. It is also desirable that the filters have boundary treatments that avoid any serious numerical artifacts so that they can be applied to many subdomains in a way that allows the constituent parts to be merged consistently back together. This is particularly important for applications to the global domain because it is difficult to apply recursive filters near the polar areas of the Gaussian grid where the curvature of the grid cannot be properly accounted for. However, by dividing the global domain into subregions furnished with their own grid, free of singularities, the recursive filter technique can be applied without difficulty to each subdomain.

In our implementation the globe is divided into three pieces: two Cartesian polar patches and a zonal band in between, and the recursive filters are applied to each subdomain. For the zonal band, both the inhomogeneity of the Gaussian grid and the shrinking of the zonal grid increments toward polar areas are treated as an equivalent-scale variation. The scale factor in the zonal direction varies as $\cos\phi$ where ϕ is the latitude. In the meridional direction, the scale factor is

$$(\phi_{j+1} - \phi_{j-1})\text{NLON}/4\pi, \tag{3.3}$$

where NLON is the number of grid points in the longitudinal direction. For the Cartesian polar patches the scale factor is

$$1/(1 + r^2), \tag{3.4}$$

where r is the distance from the pole in units of zonal grid increments at the equator.

For polar patches, the transform routine between the Cartesian grid and the lat–lon grid, and its adjoint are needed. The stereographic projection is used to project the Gaussian grid onto a plane. In the analysis procedure, the observational residual field is converted with the adjoint of the transform from the Gaussian grid to the Cartesian grid, recursive filters are applied, and the forward grid-to-grid transform is used to bring the field back to the lat–lon grid. Two blending zones between the polar patches and the zonal band allow a smooth transition when the three parts are merged back to the global Gaussian grid. Figures 3a, 3b, and 3c show, respectively, the recursive response of some randomly located impulses in two polar patches, the zonal patch, and the global field on the Gaussian grid built from the three patches without blending. The response-amplitude control is validated in the amplitudes at the center of each impulse after the filters. The response scale of the filters is designed here to be uniform on the sphere, which can be achieved by counteracting the mapping factors of the grid with scale variation on each subdomain. These counteracting factors are necessary to implement accurately the estimated scales for each variable. As shown in Fig. 3c, the contours on the boundaries of the subdomains match smoothly even without

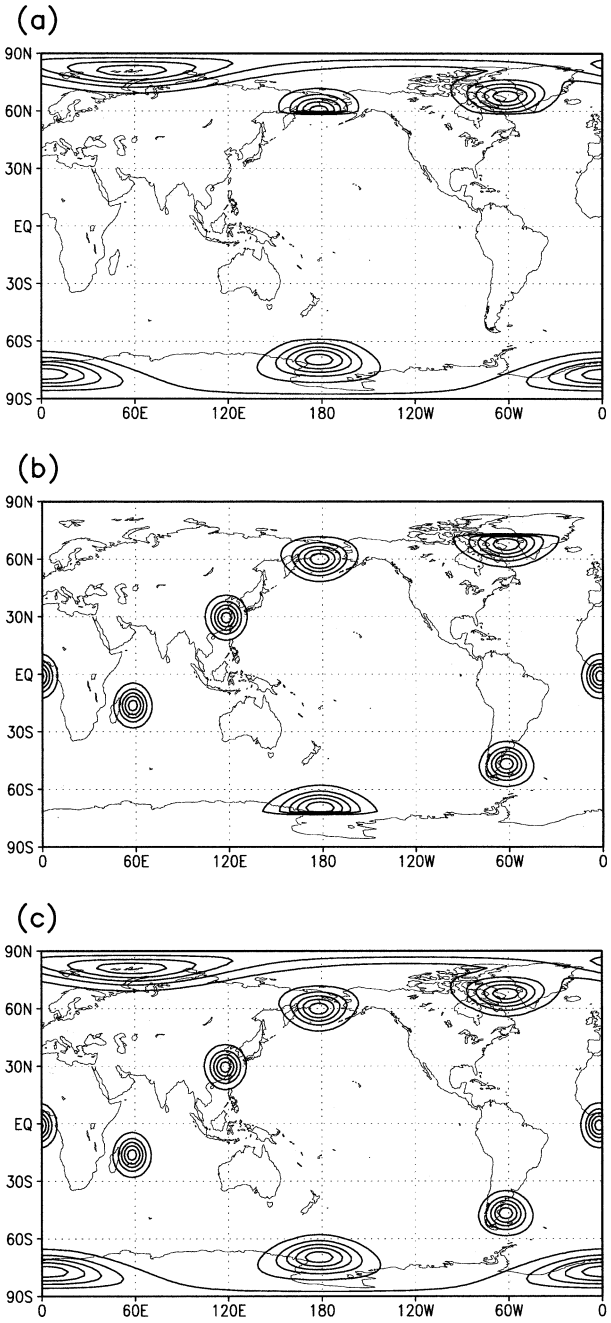

FIG. 3. Results of recursive filter on some randomly located impulses in (a) the polar patches, (b) the zonal band, and (c) merged from the subdomains without blending. The contour levels are 0.1, 0.3, 0.5, 0.7, and 0.9.

blending, which indicates that the definition of the counteracting scales in each patch is consistent, and that the boundary treatment of the recursive filters is free of numerical artifacts. If we assume that the grid is Cartesian instead of Gaussian, then the plots in Fig. 3 can be interpreted as filter results with spatially varying scales. The fact that the reconstructed global fields are almost identical with (not shown) or without blending indicates that the recursive filters meet the basic requirements.

We have observed that when the scales become very large compared to the subdomain, for example, in the stratosphere, the solutions in the buffer zone are very different for each subdomain. The resulting global field would merge from one solution to the other gradually. This is not a problem for temperature and humidity fields since the solution is constrained by the observations. But for the streamfunction and velocity potential, the forcing (wind components) of the analysis problem is the gradient of the analysis variables and the Laplacian of the variable is used as the initial condition for the forecast model. Merging the domains produces arbitrary gradients and unrealistic analysis results. The problem with large length scales is general. The reason that it is not significant elsewhere may be because the contribution from these very large scales is small in the lower levels. We solved this problem by defining the horizontal background error in spectral space for the streamfunction and the unbalanced part of velocity potential for sigma levels (pressure divided by surface pressure, as defined by Phillips 1957) above 0.15, where the characteristic spatial scales are very large. Dot products of the forcing field and diagonal background error in spectral space account for the variance and the horizontal correlation at these levels. The vertical correlation is done with recursive filters over whole fields.

4. Estimation of background error covariance

The error variance is estimated in grid space by what has become known as the NMC method (Parrish and Derber 1992; Rabier et al. 1998). The error statistics are estimated with the differences of 24- and 48-h forecasts valid at the same time for 49 cases distributed over a period of 1 yr. Both the amplitudes and the scales of the background error were tuned to represent the 6-h forecast error. The statistics that project multivariate relations among variables are used in the data assimilation as derived from the NMC method. The standard deviations of the background error for the analysis variables as functions of latitude and height are shown in Fig. 4. The amplitudes are larger in midlatitudes than in the Tropics, and larger in the Southern Hemisphere than in the Northern Hemisphere for the streamfunction, the unbalanced temperature, the unbalanced surface pressure, and the pseudo–relative humidity. The standard deviation of the streamfunction increases with height and peaks between 200 and 300 mb in most areas. The unbalanced part of the temperature has three local maxima: near the surface, around 200 to 300 mb, and near the top of the model domain. The standard deviation of the unbalanced part of velocity potential has its maximum in the Tropics and the amplitude increases with height to 150 mb, then decreases. The amplitude of the error of pseudo–relative humidity peaks around 500 mb in the midlatitudes and around 200 mb near the equator. The standard deviation of the unbalanced surface pressure has local maxima in the midlatitudes in both hemispheres.

We test two different ways of estimating the correlation length scales. The diagonal background error covariance in spectral space, estimated from the differences of 24- and 48-h forecasts, is used to retrieve the scale information. The dot product of the square root of the two-dimensional error covariance and the spectrum of a delta impulse at a given latitude was taken and the result was transferred back to the grid space. The field is then fitted with results of the recursive filters to find the scale. A range of scales that cover those found in the error statistics is divided into equally spaced small increments. The result of recursive filters for each incremental scale is used to build a table. This table is then used to find the corresponding scales of each isotropic structure in the background error statistics. The structure is fitted locally in the horizontal directions. The procedure is repeated for each variable at each latitude and height to find the horizontal scales of the structure function.

For the streamfunction, the horizontal scales can also be estimated from the variance of the vorticity and streamfunction. The formula

$$L = \left(\frac{8\mathbf{V}_{\psi}}{\mathbf{V}_{\zeta}}\right)^{1/4}$$

(see appendix) is used to find the scale of the streamfunction, where V_{ψ} is the variance of the streamfunction and V_{ζ} is the variance of the vorticity. Similarly, the variance of each variable and the variance of its second derivative are used to estimate its horizontal scales. The second derivatives are calculated in spectral space. All the variances are calculated on the grid so that the local scale information can be estimated. We find that this method produces better results than those of the previous method. Figure 5 shows the estimates of horizontal scales of the analysis variables. The horizontal scales of the streamfunction and unbalanced part of velocity potential are largest in the Tropics and the scales increase with height. The horizontal scales of temperature, surface pressure and pseudo–relative humidity are larger in the Southern than in the Northern Hemisphere but are everywhere much smaller than those of the streamfunction and velocity potential. It is found that the horizontal scales decrease when the resolution of the forecast model is increased.

The vertical scales are estimated with the vertical

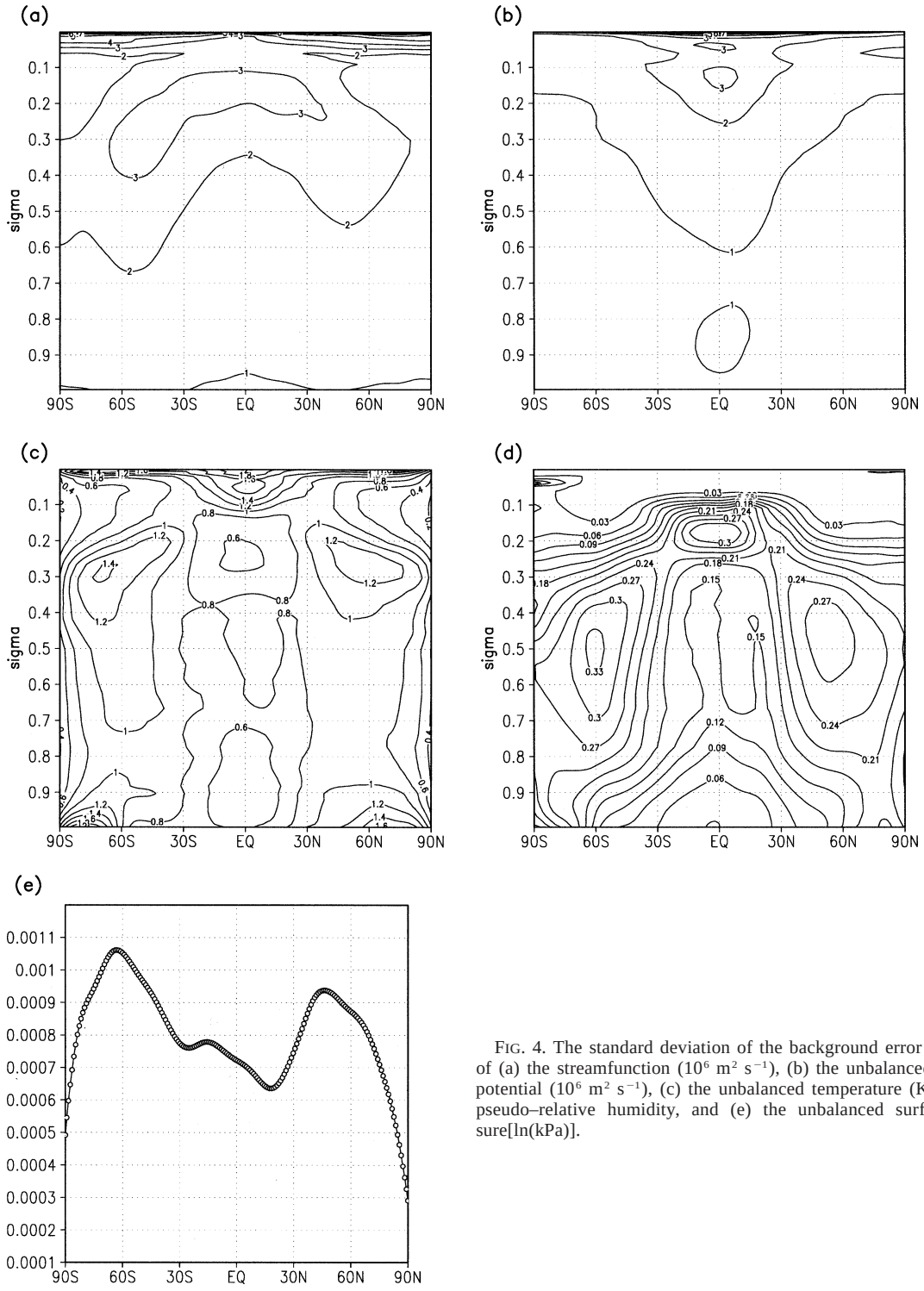

FIG. 4. The standard deviation of the background error variances of (a) the streamfunction (10^6 m^2 s^{-1}), (b) the unbalanced velocity potential (10^6 m^2 s^{-1}), (c) the unbalanced temperature (K), (d) the pseudo–relative humidity, and (e) the unbalanced surface pressure[ln(kPa)].

correlation of each variable. A second table that contains the corresponding scales and the recursive results, is built to cover the range of vertical scales. The table is used to find the scales in vertical grid units for the corresponding structures in the vertical correlation. The correlation is fitted locally in the vertical direction. The scale of the best fit from the table is assigned as the scale of the variable at that vertical level for each latitude. Note that the vertical scales are also locally defined so that the negative correlation further away in the

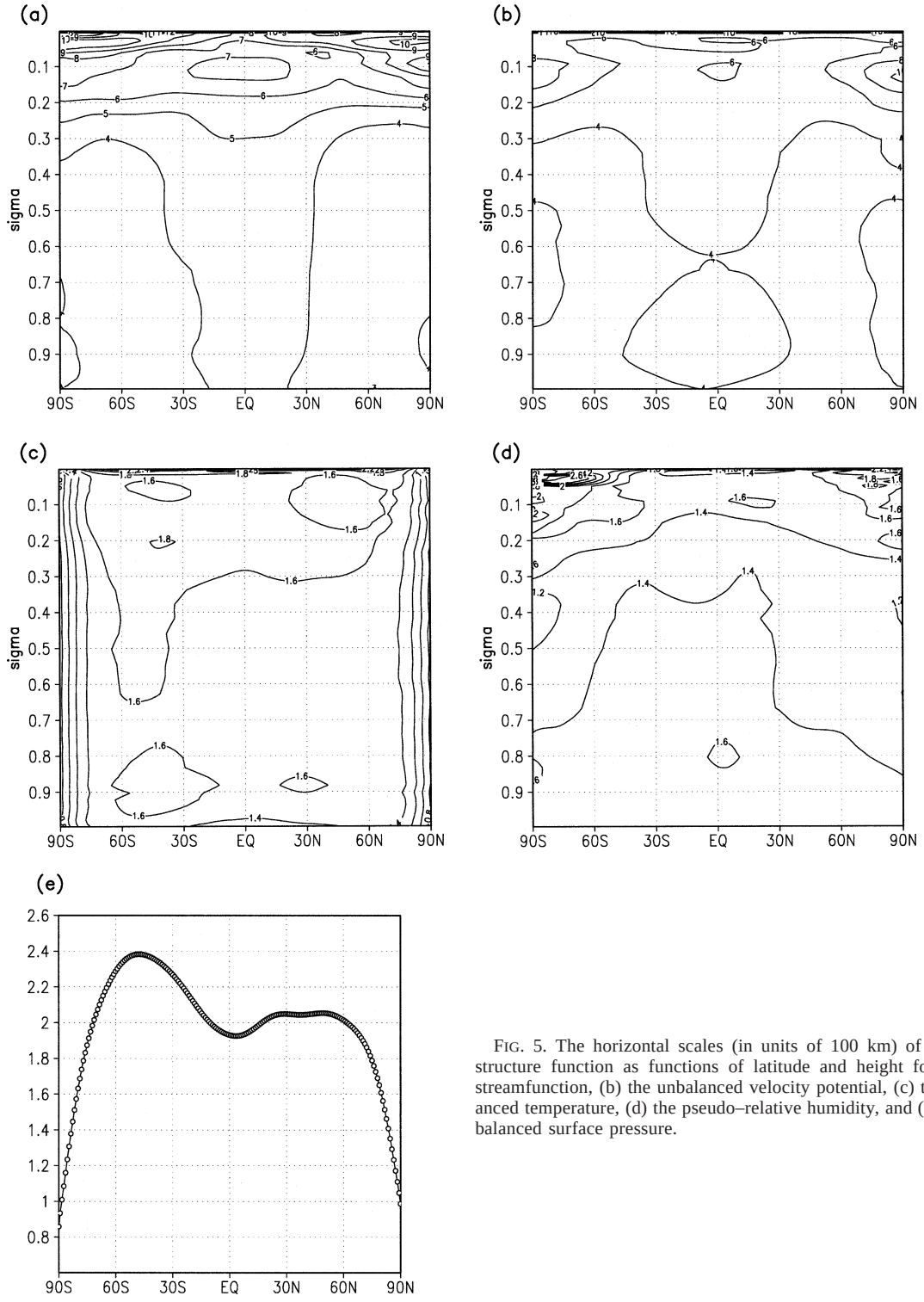

FIG. 5. The horizontal scales (in units of 100 km) of the error structure function as functions of latitude and height for (a) the streamfunction, (b) the unbalanced velocity potential, (c) the unbalanced temperature, (d) the pseudo–relative humidity, and (e) the unbalanced surface pressure.

vertical direction is not included. For unbalanced temperature, the localized vertical correlation might introduce a hydrostatic imbalance. However, we find no significant evidence of imbalance when compared with the analysis results that allow negative correlations, for example, with the analysis variables defined via coefficients of empirical orthogonal functions (EOF). For future three-dimensional anisotropic application, the localized correlation with recursive filters is chosen. Figure 6 shows the vertical scales of the error structure of

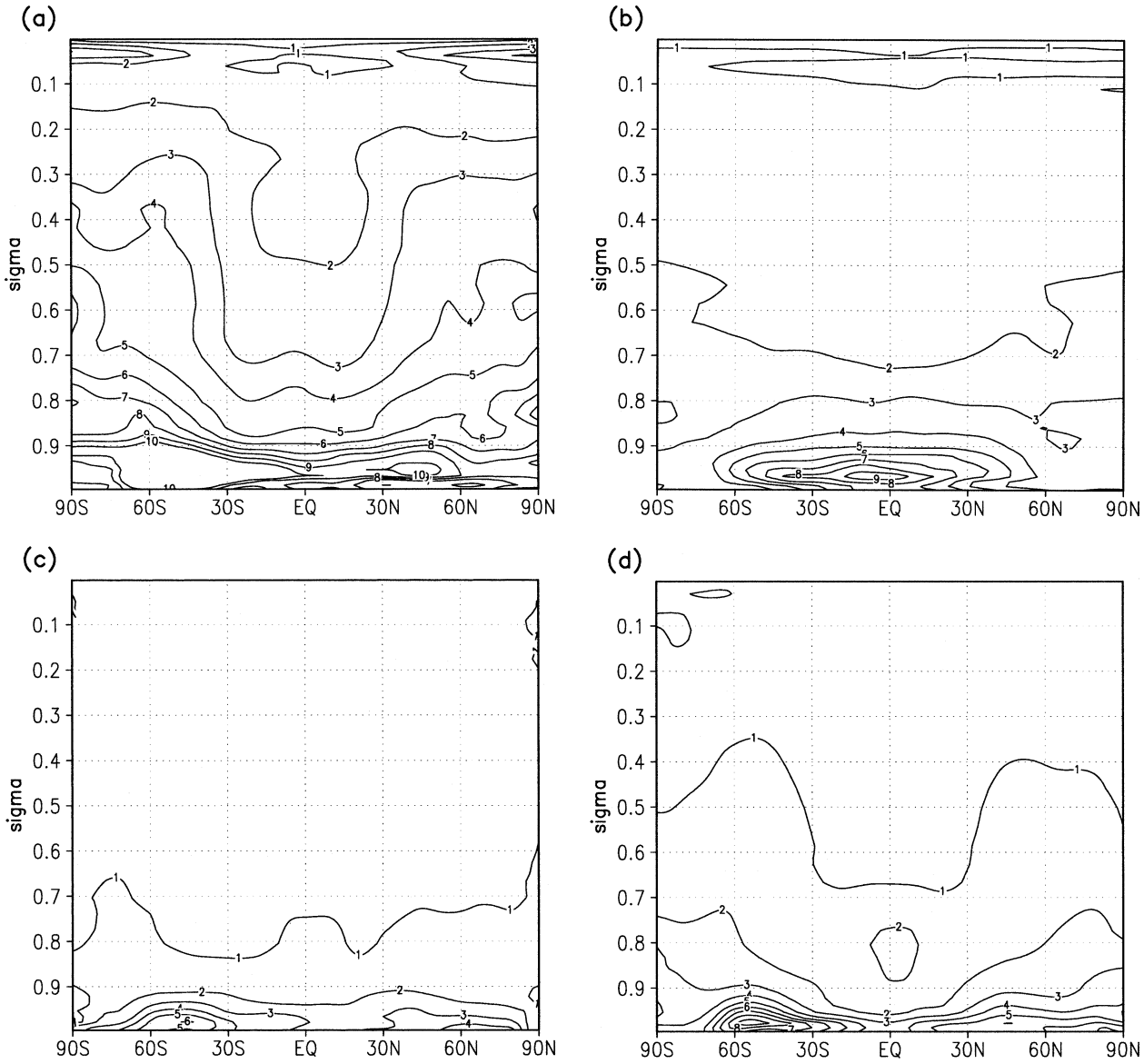

FIG. 6. The vertical scales (in units of the vertical grid) of the error structure function for (a) the streamfunction, (b) the unbalanced velocity potential, (c) the unbalanced temperature, and (d) the pseudo–relative humidity.

the analysis variables. The scales are largest near the surface boundary layer partly because of finer grid spacing. The vertical scales of the streamfunction are the largest out of all the analysis variables, followed by the unbalanced temperature. In general, the vertical scales are smaller near the Tropics than in the midlatitudes. These results are consistent with what is reported by Rabier et al. (1998) and by Ingleby (2001).

It has been recognized that objective analysis using the Gaussian shape to model the covariance severely hampers the ability of the analysis to assimilate the smallest scales. The power spectrum of a Gaussian-shaped covariance, itself being of Gaussian form, drops off faster than the spectral decay of the real atmosphere. If we assume that for small scales the background has little skill, then its error should have similar structure to the field itself (A. Lorenc 2001, personal communication). Consequently, the tails of the power spectra of the background error should be fatter (energy decreases slower) than those of any purely Gaussian spectrum. The ''fat-tailed'' feature in the spectra of error covariances is also observed when the error covariance is defined in spectral space, as in the current operational SSI. It is straightforward to apply a background error covariance with a fat-tailed spectrum in a 3DVAR that is defined in spectral space. To achieve a fat-tailed spectrum when using the recursive filters in physical space for the correlation part of the background error, a linear combination of multiple recursive filters is needed.

In our procedure, two sets of horizontal scales are

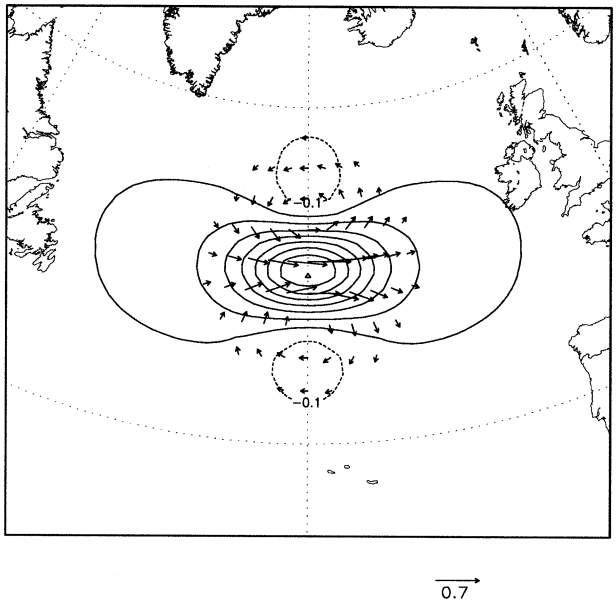

FIG. 7. The wind analysis increments in vectors superimposed on contours of *U*-component increments at sigma level 0.267, of a 1 m s^{-1} westerly wind observational residual at 50°N and 30°W at 250 mb.

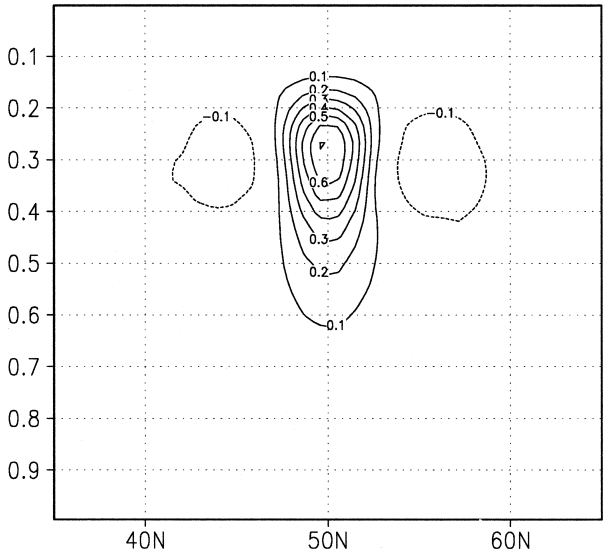

FIG. 8. Same as in Fig. 7 but the vertical cross section of the *U*-component analysis increments.

applied. The second set of the horizontal scale is set to be a half the first and the scales estimated from the NMC method fall between the scales applied. The energy of the analysis increments is projected among the scales. For use with a massively parallel processor (MPP) machine, the horizontal smoothing is done when the domain is divided into horizontal slices and the vertical smoothing is done when the domain is in vertical columns. For computational efficiency, a single recursive filter is used in the vertical direction for each variable. Nonseparability of the statistics was highlighted in the papers describing the ECMWF 3DVAR system (Courtier et al. 1998; Rabier et al. 1998; Andersson et al. 1998) with different horizontal correlations at different levels, and different vertical correlations for different horizontal wavenumbers. Our configuration only allows the specification of different horizontal scales at different levels, but not different vertical correlations for different horizontal wavenumbers. With extra sets of analysis variables, one for each of the multiple Gaussian scales (two in our setup), both scale-dependent multivariate relations and nonseparability (different vertical scale for each horizontal scale) are possible.

5. Analysis and assimilation results

The structure functions and the multivariate correlations can be visualized through the analysis increment produced by a single wind observation. Figure 7 shows, at sigma level 0.267, the wind analysis increments in vectors superimposed on contours of *u* increments, of a 1 m s^{-1} westerly wind observational residual at 50°N and 30°W at 250 mb. The uneven spacing in the increment contours shows the results of the multiscaled background error. The characteristics of the fat-tailed error covariance are shown in physical space, which allows the contour gradient to be tight when necessary, for example, dense observations, and to be loose where there is no other forcing. The vertical cross section of the analysis increment of *u*-component and projected temperature increments are shown in Figs. 8 and 9. North–south temperature gradients are induced through the multivariate correlation in the definition of the balanced part of the temperature. The changes in the mass

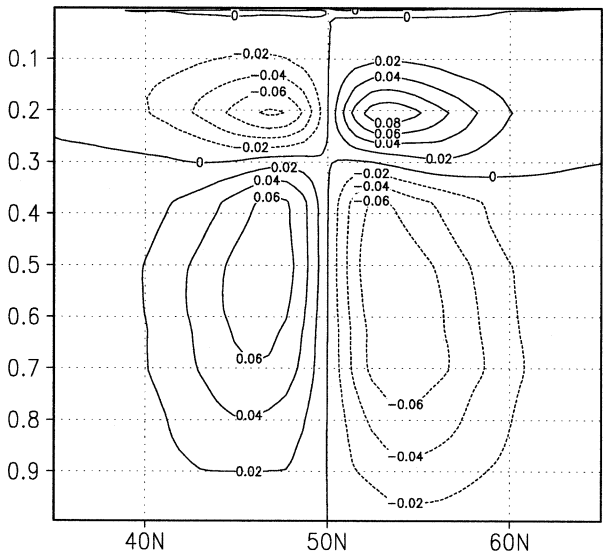

FIG. 9. Same as in Fig. 7 but the vertical cross section of the temperature analysis increments.

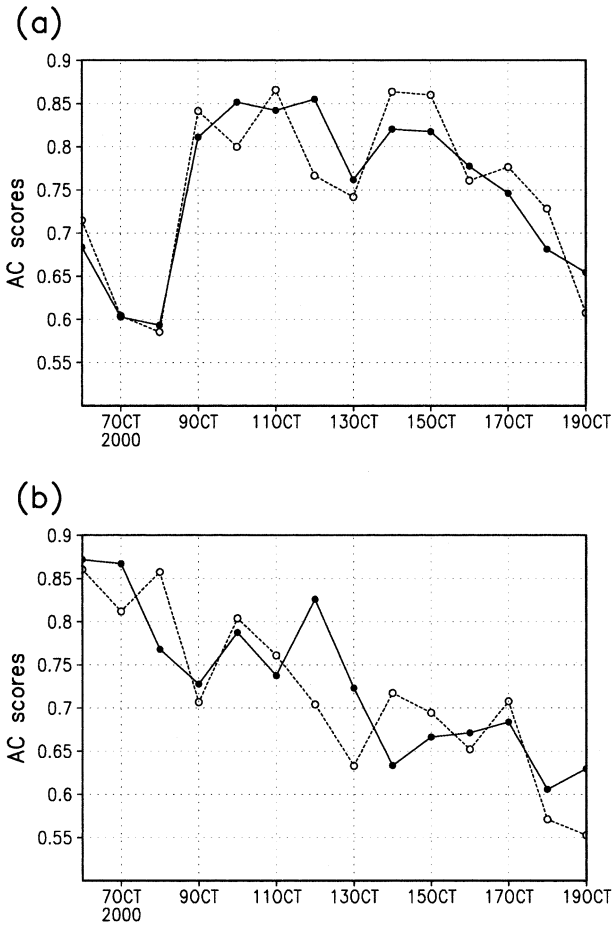

FIG. 10. Anomaly correlations in the extratropics for (a) the Northern Hemisphere and (b) the Southern Hemisphere. Solid lines are from the experiment and dashed lines are the control.

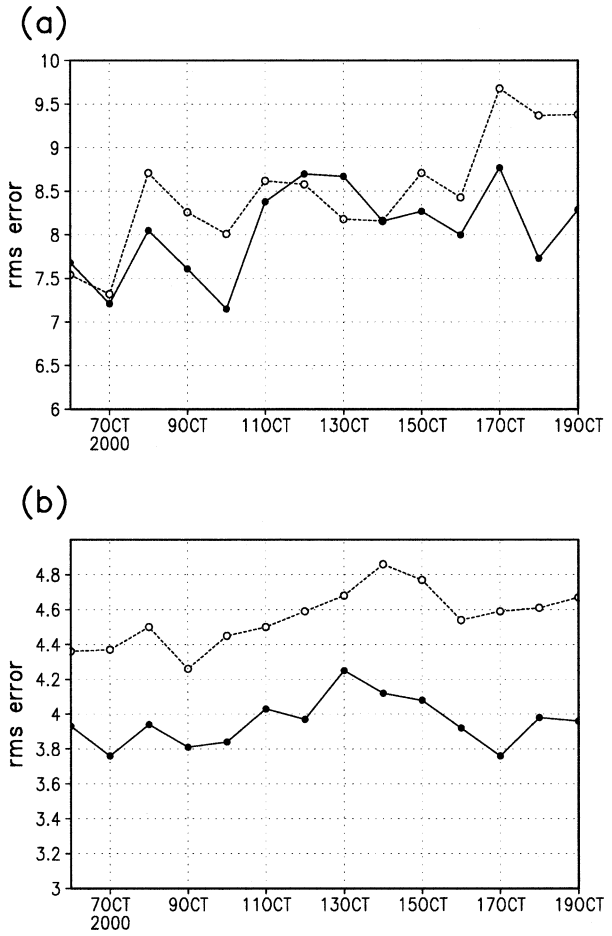

FIG. 11. Day-3 rms vector wind errors in the Tropics at (a) 200 and (b) 850 mb. Solid lines are from the experiment and dashed lines are the control.

field are stronger in amplitude and shorter in vertical scale above the forcing than below.

The analysis system is tested against the operational SSI at NCEP. Two low-resolution T62 data assimilation experiments are cycled for 19 days to produce 2 weeks of verifiable 5-day forecasts. Figure 10 shows the anomaly correlations in the extratropics (latitude 20°–80° north and south) for 500-mb height. Each experiment is verified against its own analysis. The 14-case mean for the Northern Hemisphere is 0.750 for the experiment and 0.751 for the control, and for the Southern Hemisphere the corresponding values are 0.728 and 0.716. The experimental analysis system produces neutral impact in the Northern Hemisphere and slight (1.7%) positive in the Southern Hemisphere over the 2-week period. The impact in the Tropics, however, is more consistent and positive. The day-3 root-mean-square (rms) vector wind error at 200 and 850 mb is shown in Fig. 11. The rms vector wind errors for the 200-mb wind are 8.04 m s^{-1} for the experiment and 8.50 m s^{-1} for the control, and are 3.95 and 4.55 m s^{-1} for experiment and control at 850 mb. The improvement over the period is 5.4% and 13.2% at 200 and 850 mb, respectively.

Smoother solutions have an unfair advantage when rms is used as a forecast verification statistic. The analysis increments of the *u*-component wind at 850 mb in the Tropics for the experiment and control are shown in Fig. 12. The increments in the experiment are neither smoother nor weaker than those in the control.

There are several differences between this grid space filter approach and the SSI approach. For example, the experiment employs more localized vertical correlations, thereby dropping negative correlations farther away in the vertical, and uses a mixture of the spectral approach and the model grid space filter approach. To address whether these differences lead to increased noise during the initial integration of the model, the level of initial gravity wave noise is checked through the rms divergence of the analysis and the forecast after the first time step. The results of the first and last cycles are shown in Table 1. The global rms divergence (s^{-1}) after the first time step of the forecast decreases slightly from that of the initial condition for the experiment in both

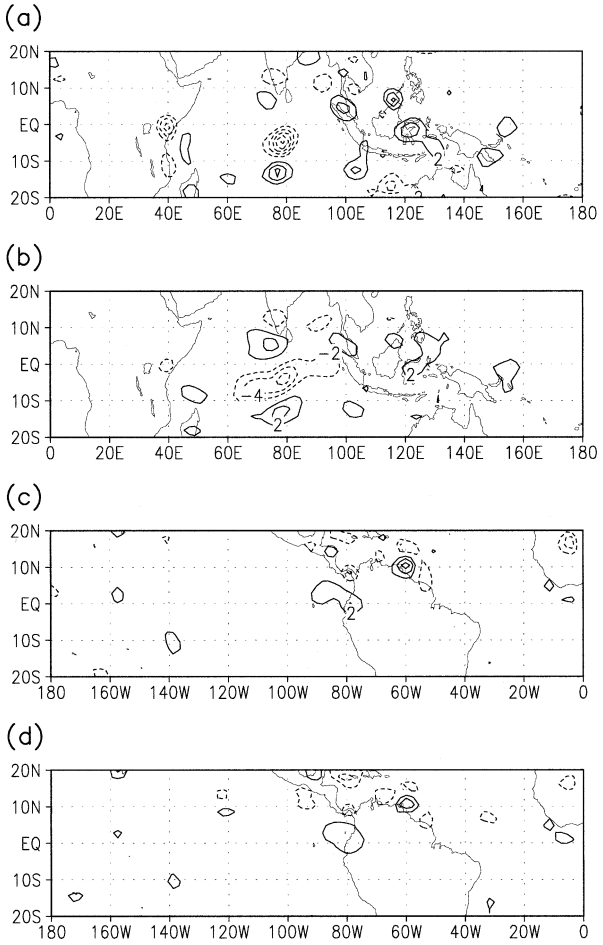

FIG. 12. Analysis increments of *U*-component wind at 850 mb in the Tropics for (a) (c) the experiment and (b) (d) the control. (a) (b) Eastern Hemisphere and (c) (d) Western Hemisphere. Contour interval is 2 m s^{-1}.

cycles, while that of the control decreases in the first cycle and increases in the last cycle. The global-mean amounts of the convective precipitation (kg m^{-2}) of the 0–3-, 3–6-, and 6–9-h forecasts averaged over the assimilation period are shown in Table 2. The two systems produce similar amounts of precipitation globally in the first 9 h of the forecasts. No evidence of excessive gravity wave adjustment and spinup in the experiment system is found.

6. Conclusions

We propose an alternative way of defining background error covariances in 3DVAR. By using recursive filters in physical space, the covariance can be made inhomogeneous. This degree of freedom comes with a price: a relatively limited freedom to specify the profile shape of the error statistics in wavenumber space. This limitation is partially overcome by applying multiple recursive filters for the structure functions.

In the experiments the error structures are kept similar to those in NCEP's SSI since the scales of the background error structures are estimated by the NMC method and are assumed to be homogeneous, at least in the zonal direction. The small impact in the extratropics indicates that 3DVAR formulated in physical space can be as effective as in spectral space. The consistent positive impact in the Tropics indicates that the newly gained freedom in the background error's spatial variation (latitude dependence in the current setup) is beneficial to forecasts compared with the greater freedom in wavenumber space (as in the SSI) in which the statistics represent the global characteristics lacking any spatial modulation.

Cutting up the global domain for recursive filters has limitations. The problem is more severe in stratospheric layers where the scales of the structure function are about as large as the subdomain dimensions. The current solution is to apply the horizontal background error of the streamfunction and velocity potential in spectral space at those vertical levels where this problem arises.

It is straightforward to apply this physical-space 3D variational analysis to a regional domain. The system is planned to be tested for operational implementation in NCEP. For future work we plan to develop a fully inhomogeneous and anisotropic background error covariance in the system using a new extension of the recursive filtering technique, which is briefly described in Purser et al. (2002b, manuscript submitted to *Mon. Wea. Rev.*).

TABLE 1. Global rms divergence (s^{-1}) of the analysis and the forecast after the first time step.

	Analysis_1	Forecast_1	Analysis_2	Forecast_2
Experiment	8.593e-6	8.361e-6	8.763e-6	8.583e-6
Control	8.082e-6	7.962e-6	7.644e-6	7.966e-6

TABLE 2. Global-mean convective precipitation (kg m^{-2}) averaged over the assimilation period.

	0–3 h	3–6 h	6–9 h
Experiment	0.2443	0.2331	0.2459
Control	0.2449	0.2363	0.2449

Acknowledgments. The authors would like to thank Drs. Roger Daley, Dick Dee, John Derber, Bruce Ingleby, Andrew Lorenc, Russ Treadon, Frances Verter, Dusanka Zupanski, and Milija Zupanski for many helpful discussions and the reviewers for their invaluable comments. We would also like to thank Prof. Eugenia Kalnay and Dr. Steven Lord for their encouragement and support. This work was partially supported by the NSF/NOAA Joint Grants Program of the U.S. Weather Research Program. This research is also in response to requirements and funding by the Federal Aviation Administration (FAA). The views expressed are those of the authors and do not necessarily represent the official policy or position of the FAA.

APPENDIX

Derivation of Horizontal Correlation Length

The following is a derivation of the formula used to obtain horizontal correlation length estimates using the ratio of variance of a field with variance of the Laplacian of the field. Using streamfunction as an example, let the streamfunction error covariance be defined as

$$\mathbf{C}_{\psi_1\psi_2} = \mathbf{V}_\psi XY$$

where

$$X = \exp\left(-\frac{1}{2}\alpha\delta^2\right); \qquad Y = \exp\left(-\frac{1}{2}\alpha\varepsilon^2\right), \quad \text{and}$$

$$\alpha = L^{-2}; \qquad \delta = x_1 - x_2; \qquad \varepsilon = y_1 - y_2.$$

The variance $\mathbf{V}_\psi$ is assumed to be constant. Here, (x_1, y_1) and (x_2, y_2) are the coordinates of the two points being correlated.

Then the vorticity covariance is given by

$$\mathbf{C}_{\zeta_1\zeta_2} = \nabla_1^2\nabla_2^2\mathbf{C}_{\psi_1\psi_2'}$$

which yields upon completing the differential operators,

$$\mathbf{C}_{\zeta_1\zeta_2} = 8\alpha^2\mathbf{V}_\psi XY\left[1 - \alpha(\delta^2 + \varepsilon^2) + \frac{\alpha^2}{8}(\delta^2 + \varepsilon^2)^2\right].$$

The vorticity variance $\mathbf{V}_\zeta = \mathbf{C}_{\zeta_1\zeta_2}$ for $\delta = \varepsilon = 0$ is given by

$$\mathbf{V}_\zeta = 8\alpha^2\mathbf{V}_{\psi'}$$

and finally, using $\alpha = L^{-2}$ we have for the correlation length estimate, given the vorticity and streamfunction variances,

$$L = \left(\frac{8\mathbf{V}_\psi}{\mathbf{V}_\zeta}\right)^{1/4}.$$

REFERENCES

Andersson, E., and Coauthors, 1998: The ECMWF implementation of three-dimensional variational assimilation (3D-Var). III: Experimental results. *Quart. J. Roy. Meteor. Soc.*, **124,** 1831–1860.

Courtier, P., and Coauthors, 1998: The ECMWF implementation of three-dimensional variational assimilation (3D-Var). I: Formulation. *Quart. J. Roy. Meteor. Soc.*, **124,** 1783–1807.

Dee, D. P., and A. M. Da Silva, 2002: The choice of variable for atmospheric moisture analysis. *Mon. Wea. Rev.*, in press.

Derber, J., and A. Rosati, 1989: A global oceanic data assimilation system. *J. Phys. Oceanogr.*, **19,** 1333–1347.

Desrozier, G., 1997: A coordinate change for data assimilation in spherical geometry of frontal structures. *Mon. Wea. Rev.*, **125,** 3030–3038.

Gill, P. E., W. Murray, and M. H. Wright, 1981: *Practical Optimization.* Academic Press, 401 pp.

Gustafsson, N., and Coauthors, 1999: Three-dimensional variational data assimilation for a high resolution limited area model (HIRLAM). Swedish Meteorological and Hydrological Institute Tech. Rep. 40, 74 pp.

Hayden, C. M., and R. J. Purser, 1995: Recursive filter objective analysis of meteorological fields: Applications to NESDIS operational processing. *J. Appl. Meteor.*, **34,** 3–15.

Ide, K., P. Courtier, M. Ghil, and A. C. Lorenc, 1997: Unified notation for data assimilation: Operational, sequential and variational. *J. Meteor. Soc. Japan*, **75,** 181–189.

Ingleby, N. B., 2001: The statistical structure of forecast errors and its representation in the Met Office global 3-dimensional variational data assimilation scheme. *Quart. J. Roy. Meteor. Soc.*, **127,** 209–232.

Navon, I. M., and D. M. Legler, 1987: Conjugate-gradient methods for large-scale minimization in meteorology. *Mon. Wea. Rev.*, **115,** 1479–1502.

Parrish, D. F., and J. C. Derber, 1992: The National Meteorological Center's spectral statistical-interpolation analysis system. *Mon. Wea. Rev.*, **120,** 1747–1763.

Phillips, N. A., 1957: A coordinate system having some special advantages for numerical forecasting. *J. Meteor.*, **14,** 184–185.

Purser, R. J., and R. McQuigg, 1982: A successive correction analysis scheme using recursive numerical filters. Met O 11 Tech. Note. 154, British Meteorological Office. 17 pp.

Rabier, F., A. McNally, E. Anderson, P. Courtier, P. Unden, J. Eyre, A. Hollingsworth, and F. Bouttier, 1998: The ECMWF implementation of three-dimensional variational assimilation (3D-Var). II: Structure functions. *Quart. J. Roy. Meteor. Soc.*, **124,** 1809–1829.

Riishojgaard, L. P., 1998: A direct way of specifying flow-dependent background correlations for meteorological analysis systems. *Tellus*, **50A,** 42–57.

Weaver, A., and P. Courtier, 2001: Correlation modelling on the sphere using a generalized diffusion equation. *Quart. J. Roy. Meteor. Soc.*, **127,** 1815–1846.